45th AIAA/ASME/SAE/ASEE Joint Propulsion Conference & Exhibit
2 - 5 August 2009, Denver, Colorado

AIAA 2009-5164

Propagation of Swirl in Transonic Airflow

A. Abdelhafez* **and A. K. Gupta†**
Department of Mechanical Engineering, University of Maryland
College Park, MD 20742

The propagation of swirl and the choking criteria of swirling transonic airflow are examined both numerically and experimentally in underexpanded airflow at matched nozzle reservoir pressure as well as matched mass flow. It was found that the swirl number is not conserved in the expanding subsonic flowfield inside nozzle but decreases as the throat is approached. It was also found that the throat velocity itself (not any of its components) is choked in a swirling flowfield. Therefore, the application of swirl always results in a reduction in axial Mach number component. Since the mass flow through nozzle is a function of throat density and axial Mach number, the reduction in the latter with swirl explains the observed reduction in mass flow (discharge coefficient) at matched nozzle reservoir pressure. Greater reservoir pressures, on the other hand, result in higher throat densities, which compensates for the reduced axial Mach number, and the mass flow rate can be matched its non-swirling value. It was also found that the distribution of subsonic Mach number (not any of its components) in a swirling flow is solely dependent on cross-sectional area, similar to non-swirling flows, i.e., non-swirling and swirling flows have the same subsonic Mach number profile. The supersonic swirl number was found to experience a slight local increase within shock structure, where the axial momentum undergoes significant reduction, whereas the tangential one is preserved and experiences no change.

Downloaded by UNIVERSITY OF MARYLAND on September 7, 2014 | http://arc.aiaa.org | DOI: 10.2514/6.2009-5164

Nomenclature

A	=	cross-sectional area
D	=	nozzle-exit diameter (11 mm)
M	=	Mach number
$\dot{m}$	=	mass flow rate
p	=	pressure
R	=	specific gas constant
r	=	radial coordinate
S	=	swirl number
T	=	temperature
v	=	velocity
z	=	axial coordinate
γ	=	ratio of specific heats
ρ	=	density
Subscripts		
a	=	axial
t	=	tangential

I. Introduction

Hypersonic vehicles, powered by scramjet engines, are pivotal for the future of high-speed flight. The critical science issues in hypersonic research under in-flight conditions have not been fully understood yet. These issues include mixing in supersonic airbreathing engines. It is desired to maintain supersonic flow through the combustor of a scramjet engine, in order to reduce the losses in total pressure and temperature inherent in decelerating the flow to subsonic speeds. Extensive investigations are still needed in order to achieve better understanding of the complicated flow dynamics and chemistry involved with the final goal of improved efficiency and performance. Successful operation of any air-breathing system depends primarily on efficient mixing of the injected fuel with airflow. The efficiency of an injection system is defined by the achievable degree of fuel/air mixing. Supersonic flows are compressible and resistant to fuel penetration and mixing. Therefore, the equivalence ratio of scramjet-engine operation has to be fuel-rich over a considerable part of the vehicle flight, in order to ensure that a flame is present to provide positive thrust. Any progress made on improving the engine efficiency must, therefore, be closely followed towards achieving efficient mixing between fuel and air. Scramjet flows have residence times of the order of only few milliseconds. In this short residence time, one must account for the mixing, ignition delay, and combustion time scales.

Swirl is one of the solutions of interest to the problem of poor supersonic mixing. The mixedness of a supersonic fuel jet injected into the supersonic airflow of a scramjet engine can be improved by imparting swirl to the fuel jet. This is achieved practically by tangential injection of fuel into its plenum and allowing the flow to accelerate through a nozzle. In other words, a subsonic swirling flow accelerates to supersonic speeds in a choked nozzle. Swirling compressible flows occur also in a variety of other practical applications, including turbofans and turbojet engines, integral rocket/ramjets, fluidic vortex valves. In the first case, the tangential velocity component is induced by the motion of turbine blades. For ramjets, experimental studies have demonstrated that the swirl generated by fixed vanes located in the dump combustor inlet can lead to significantly improved combustor performance.[1] Clearly, the generated swirl in each of those propulsion systems will persist at some level to the

* Graduate Student, Student Member AIAA
† Distinguished University Professor, Fellow AIAA, akgupta@umd.edu

Copyright © 2009 by the Authors. All rights reserved. . Published by the American Institute of Aeronautics and Astronautics, Inc., with permission.

inlet of exhaust nozzle. The behavior of a transonic swirling flow is thus of practical importance, which motivated this current study to examine the effect of axisymmetric vorticity on nozzle flowfield, so that design parameters such as thrust and mass flow rate can be accurately determined.

Subsonic swirling flows have been examined extensively in the literature, but little of fundamental nature is known of the supersonic ones. Quasi-one-dimensional theory apply very well as a first approximation in non-swirling supersonic flowfields, but previous attempts to extend those theory to swirling supersonic flows have all failed, due to the intrinsic three-dimensionality of such flows. The most fundamental problem is the identification of choking criterion. One-dimensional theory without swirl prove that the throat Mach number is unity, implying that the mass flux through the throat of a fixed-geometry nozzle is maximum, and that the throat velocity is equal to the speed of sound. The first criterion of maximum mass flux can be carried over to the swirling flowfield with known stagnation conditions. It is still not clear, however, how the second criterion applies to choked swirling flows. Because of the non-uniform throat velocity distribution, it is difficult in the absence of CFD numerical simulations to predict which velocity or velocity component is equal to the local speed of sound. The maximum-mass-flux criterion has been used by several investigators. It was originally introduced by Mager[2] in his theoretical study of choked free-vortex flows with the ratio of specific heats $\gamma = 1.40$. His results were extended by Swithenbank and Sotter[3] to the case of $\gamma = 1.25$, while Glick and Kilgore[4] presented results for γ in the range 1.10 – 1.28.

The analysis of the free-vortex case is simplified by the fact that it is a potential flow, whereas the forced-vortex flow is truly rotational. This may be the reason why there have been several unsuccessful attempts to derive analytical expressions for the output characteristics of nozzles with choked flows. Bastress[5] tried to use the sonic velocity criterion by incorrectly assuming that the velocity magnitude was constant across each section and equal to the critical velocity at the throat. In addition, he assumed forced-vortex flow at all stations. Manda[6] used the constant-stagnation-enthalpy assumption to derive an equation for the axial velocity. Forced-vortex flow was again assumed at all stations, but this time the equality of velocity magnitude and critical velocity at throat was assumed to be satisfied only on the nozzle axis at the throat. King[7] proposed another solution in which he pointed out that the assumption of forced-vortex flow cannot hold everywhere, as it renders the problem over-specified. Manda,[8] however, showed that King's solution violated the radial momentum equation. Finally, all the preceding articles were summarized and discussed by Hsu[9] who concluded that the basic reason behind the controversy lies in the fact that the one-dimensional approximation could not be applied to swirling flows.

Lewellen et al.[10] developed an approximation that can be used to determine how swirl affects the choking constraint on flow through the throat of a nozzle. It was found that the mass flow rate through a choked nozzle can be sharply reduced by introducing a tangential component of velocity into the flow. Moreover, the choking constraint imposes a limit on the maximum tangential Mach number that can be achieved in a vortex tube, even when an infinite pressure ratio is available. The theoretical choking constraint was used to speculate on the limiting tangential Mach number. It was concluded that this limiting value is 1.2, which is consistent with the experimental observations of Roschke and Pivirotto[11] who reported a value of 1.05. Toomre[12] achieved a value of 1.03, independent of mass flow rate, and Pinchak and Poplawski[13] reported a value of 1.18.

The lack of comprehensive understanding of supersonic swirling flows has also led to a controversy in terms of nozzle thrust and specific impulse. While some studies showed that the discharge coefficient, thrust, and specific impulse decrease with swirl, others reported that thrust can be increased with swirl. It is thus of fundamental as well as practical importance to determine how the nozzle propulsive characteristics are affected by the application of swirl.

Batson and Sforzini[14] studied the structure of swirling flow through a convergent nozzle with emphasis on the effect of swirl on flowfield, thrust, and mass flow produced by nozzled devices, such as jet engines and spin-stabilized rockets. It was reported that the axial velocity component increases, whereas the tangential one decreases, as the flow passes through nozzle throat. In another study, which has application in ramjets and turbojets, Kornblum et al.[15] presented an analytical performance prediction methodology for annular propulsive nozzles, with swirl introduced in the combustor upstream of nozzle. This methodology was applied to a specific nozzle design for a free-vortex swirl distribution. The results showed that the discharge coefficient, thrust, and specific impulse decrease as the amount of swirl is increased. Application of the prediction methodology to swirl distributions other than free vortex was recommended for future work. Hoffman et al.[16] followed this recommendation by applying this methodology to examine the effects of swirler design on nozzle performance. Four types of swirlers were investigated, namely free-vortex, constant-angle, forced-vortex, and Rankine-vortex swirlers. The computed results indicated again that swirl decreases the discharge coefficient, thrust, and vacuum specific impulse. The decrease in discharge coefficient correlates with the mass-averaged swirl for all four types of swirlers. The decrease in vacuum specific impulse is, on the other hand, a function of swirler design. Forced-vortex swirlers induce the least reduction in specific impulse, whereas free-vortex ones induce the greatest reduction.

The present work provides a numerical/experimental investigation of the propagation of swirl and the choking criteria in swirling transonic airflow. This problem is still not fully understood due to its intrinsic three-dimensional nature. Answers are provided for fundamental questions, such as: Is

Downloaded by UNIVERSITY OF MARYLAND on September 7, 2014 | http://arc.aiaa.org | DOI: 10.2514/6.2009-5164

the throat velocity (or any of its components) equal to the local speed of sound in a swirling flowfield? How does swirl affect the throat Mach number, pressure, and temperature? How different are the axial variations of supersonic and subsonic swirl number?

II. Experimental Setup

The experimental investigation of this present work has been performed on the UMD supersonic facility. The utilized supersonic-nozzle assembly is shown schematically in Figure 1. A convergent nozzle of inlet-to-exit area ratio of 25 is used to generate an underexpanded supersonic airflow. Reservoir pressures of up to about 9 atm (abs) are available, yielding near-field Mach numbers of up to 2.2 under non-swirling conditions. The nozzle has swirling capabilities, wherein the axial-tangential-entry technique with four tangential inlets is utilized to accurately control the degree of swirl imparted to airflow. This technique has been proven in previous research to be an efficient method for generating supersonic swirling jets.[17–19] Thermal flow meters/controllers are used to meter the flow rates of axial and tangential air components with an accuracy of ±1.5% full-scale.

The nozzle was machined out of a single aluminum rod. Aluminum was preferred to stainless steel because the former has higher thermal conductivity, which prevents overheating of nozzle walls during combustion experiments. The higher conductivity allows radiated heat to be dissipated effectively through the thick nozzle walls. The dissipated heat is removed by forced convection of the entrained ambient cold air through the large surface area of nozzle external walls. The thickness of nozzle lip was optimized to allow for significant entrainment of ambient air while having adequate rigidity for machining the exit section to the desired surface finish and dimensional tolerance.

The nozzle is equipped with a coaxial fuel-injection system to provide the ability to inject fuel along nozzle axis, if needed. A support flange upstream of nozzle maintains concentricity of the injection system, especially under swirling conditions. This flange comprises a conical sleeve that embraces the injection system. The sleeve wall-thickness decreases in the direction of flow to prevent any blockage close to the nozzle exit. Three spokes extend to the support flange to hold the sleeve in place. The spokes are located physically upstream of air tangential inlets and do not affect the flowfield of tangential air component. The supersonic flow exiting the nozzle was examined using Schlieren imaging and found to be fully axisymmetric with and without swirl.

Nozzle thrust was measured experimentally to assess the effect of swirl and provide validation for the numerical results. In order to measure the thrust, the nozzle assembly was connected to a compression load cell (transducer) of 200-N capacity and ±0.5% FSO accuracy.

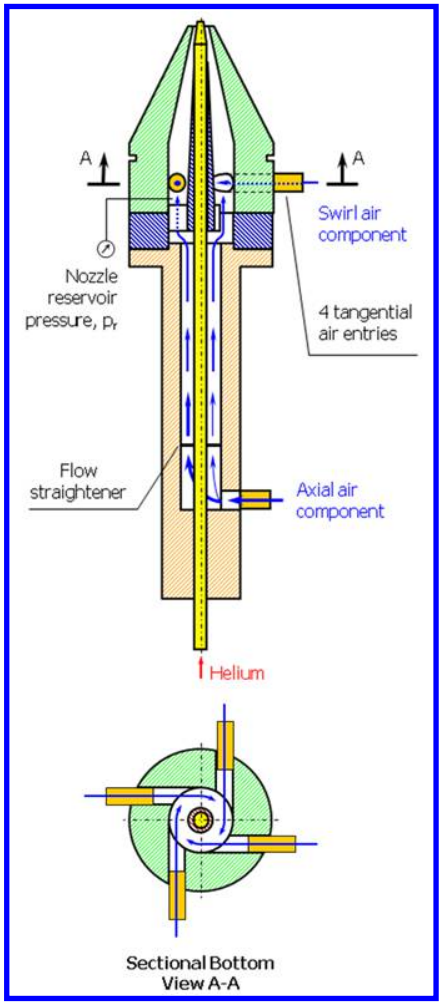

Figure 1. Schematic of UMD supersonic-nozzle assembly

III. Numerical Simulation Assumptions

The ESI-Group CFD-FASTRAN 2008 LES-based code was used for all the simulations conducted in this study. A variable-size grid was generated for the examined geometry. Tighter meshing was implemented near and at the critical geometry locations, e.g., the exits of nozzle and fuel-injection system. Special emphasis was placed on the level of cell skewness. The geometry was sub-divided into individual volumes, each meshed separately, in order to keep the skewness level of the most skewed cell below 0.5. Mesh dependence was carefully examined through testing multiple levels of mesh tightness. A total of 7,166,860 nodes were found sufficient. Higher tightness levels did not yield any significant changes in the obtained profiles and were thus not considered, in order to optimize the computational time.

The Baldwin-Lomax turbulence model was implemented.[20] Calculation of viscosity and conductivity was based on the kinetic theory of gases. The mass diffusivity was calculated using Fick's law with a Schmidt number of 0.5. A turbulent

Downloaded by UNIVERSITY OF MARYLAND on September 7, 2014 | http://arc.aiaa.org | DOI: 10.2514/6.2009-5164

Prandtl number of 0.9 was used for calculating the turbulent conductivity. Similar to the experimental conditions, the total temperature at air inlets was kept fixed at 300 K, while the total pressure was maintained at 7.91 bar without swirl and 8.82 bar with swirl. The 8.82-bar value was carefully chosen to ensure a common air flow rate of 175 g/s. (The need for higher nozzle reservoir pressure with swirl is explained in detail in the 'Results and Discussion' section.) The total pressure and temperature at air inlets were preserved throughout the iteration process in each examined case, until convergence was attained. Owing to the relatively large cross-sectional areas of the air inlets, the entrance Mach number of air was only about 0.02, resulting in almost identical inlet stagnation and static conditions.

The nozzle walls were set to be isothermal at 280 K, based on multiple temperature measurements of the nozzle interior and exterior walls. This is attributed to the aforementioned fact that the nozzle is made of aluminum, which has a high thermal conductivity and thus allows the nozzle to act as a near-isothermal body. The walls of fuel-injection system, on the other hand, were set to be adiabatic, because the injection system is immersed almost totally into the nozzle and conditioning chamber, which allows for negligible amounts of heat to be conducted axially upstream through the thin walls of fuel system. Moreover, it is made of stainless steel that has a lower thermal conductivity (relative to aluminum).

Since the simulation involves a free supersonic flow, special emphasis was placed on the choice of boundary conditions that represent the flow surroundings. The entire nozzle assembly was surrounded by a cylindrical enclosure of (40 D) diameter and (70 D) length, where D is the nozzle exit diameter (11 mm) — a good representative of jet size. The 40-D enclosure diameter assures that the side boundaries are far enough, in order to eliminate any interference with the jet and to maintain near-stagnation atmospheric properties at the boundaries. Consequently, the bottom and side enclosure surfaces were fixed-pressure boundaries. The top side of enclosure, on the other hand, is an outlet located 55 D away from the nozzle exit (≈ 78% of the 70-D enclosure length). This guarantees that the flow leaves the simulated geometry shock-wave-free, since it was observed with Schlieren imaging that complete transition to subsonic speeds occurs about 30 D downstream of nozzle exit.

The initial conditions of simulation were set for all cases at 1-atm static pressure, 300-K static temperature, 9.7-m/s axial velocity, and zero radial and tangential velocities. Consequently, the simulation incorporated the transient flow behavior as the high-pressure air expands and "marches" from geometry inlet to exit. An initial CFL (Courant–Friedrichs–Lewy) number[21] of 0.1 was chosen that increases to unity as convergence is approached. Time integration is implicit, where the Point Jacobi (fully implicit) scheme was used. Backward Euler discretization was implemented. Each iteration included 20000 sub-iterations. Convergence was usually attained after 18500 – 19500 iterations.

IV. Test Matrix

The effect of swirl is investigated here by forwarding the entire airflow to nozzle tangential entries. This allows for examining a single degree of swirl, namely the maximum attainable one. Consequently, the swirling cases of this study have a common nozzle-based geometrical swirl number of 0.68. The term "nozzle-based" refers to nozzle operation in the absence of coaxial injection system, as it will be shown later that the presence of this system reduces the geometrical swirl number down to 0.36.

The total pressure and temperature of air were kept constant at 7.91 bar and 300 K, respectively, for the non-swirling case presented here, which resulted in an air flow rate of 175 g/s. It was noticed, however, that imparting swirl to airflow at the same nozzle reservoir pressure of 7.91 bar results in reduced mass flow rate through the nozzle. This observation agrees with the findings of many previous studies (see the preceding literature review), where it was proven that imparting swirl to the airflow results in "additional choking" of the nozzle, i.e., a lower mass flow rate compared to the corresponding non-swirling conditions at the same reservoir pressure. (A theoretical limit of no flow was even predicted at an infinitely large swirl number.) Therefore, a higher reservoir pressure is necessary to maintain the same flow rate through the nozzle. It was found in this study that a value of 8.82 bar yields identical air flow rates of 175 g/s in the non-swirling and swirling cases.

Table 1 lists the cases examined here. Case 1 is a non-swirling reference case. Cases 2 and 3, on the other hand, are swirling cases. The former represents the application of swirl at matched-mass-flow conditions, while the latter represents matched nozzle reservoir pressure.

V. Results and Discussion

Validation of Numerical Code

Code validation is demonstrated here by comparing the experimentally measured thrust values to the numerically computed ones. They differ by only 0.6 – 3.2%, which shows very good agreement and confirms the capability of numerical code to quantify the subsonic and throat flows with high accuracy.

Table 1. Test Matrix

Air total temperature at inlet = 300 K (constant)

Case	Reservoir pressure [bar]	$\dot{m}$ [kg/s]	S_g
1	7.91	0.175	0
2	8.82	0.175	0.36
3	7.91	0.150	0.36

Downloaded by UNIVERSITY OF MARYLAND on September 7, 2014 | http://arc.aiaa.org | DOI: 10.2514/6.2009-5164

Downloaded by UNIVERSITY OF MARYLAND on September 7, 2014 | http://arc.aiaa.org | DOI: 10.2514/6.2009-5164

Subsonic Propagation of Swirl

Since the examined nozzle involves a non-recessed coaxial injection system, the effect of its presence on nozzle performance is analyzed first. It was shown in earlier research that the presence of a coaxial needle inside nozzle affects the airflow properties.[22] Figure 2 shows the axial variation of subsonic swirl number inside nozzle in the absence as well as presence of the coaxial injection system. Using the same conditions of case 2 in Table 1 (injection system present, no fuel injection), another case was simulated with the injection system absent. The swirl number was computed at select sections inside the nozzle using the correlation[17]

$$S = \frac{\int_{R_i}^{R_o} v_a \, v_t \, r^2 \, dr}{R_o \int_{R_i}^{R_o} v_a^2 \, r \, dr}$$

where v_a and v_t are the numerically-obtained axial and tangential velocity components, respectively. Multiple observations can be made from Figure 2. The most obvious and expected one is that the swirl number decreases, as flow progresses towards nozzle throat. This agrees with the findings of Linck[19] and can be attributed to two facts: (a) v_a increases substantially due to flow expansion and acceleration, and (b) v_t was observed to decrease slightly due to viscous losses, as the flow passage narrows and boundary layers develop at the walls. It is worth noting that the swirl number can be roughly approximated as being proportional to the ratio of average tangential to axial components (neglecting the effect of nozzle geometry), which explains the trends depicted in Figure 2.

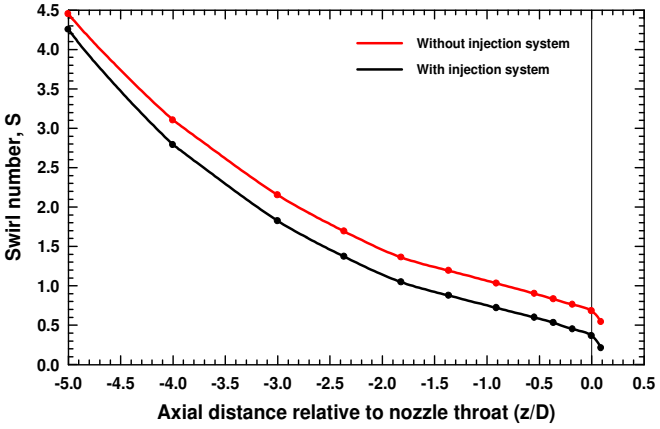

Figure 2. Axial variation of subsonic swirl number inside nozzle in the absence (red) and presence (black, case 2) of coaxial injection system. Nozzle throat at z/D = 0

Figure 2 also reveals that the presence of injection system induces an additional reduction in swirl number throughout the entire nozzle. This is attributed to the development of a second boundary layer along the injection-system walls. Close to the plane of tangential inlets, the relative reduction is small but keeps increasing as the flow progresses through nozzle. This statement is concurred by Figure 3, where the relative reduction in swirl number is plotted. While the upstream sections experience minor reductions, a 47% reduction from 0.68 to 0.36 exists at the nozzle throat due to the presence of injection system, which blocks 17% of throat area. The significant reduction in throat swirl number is further explained in Figure 4. Shown is the radial variation of tangential Mach number at z/D = –0.1 in the absence and presence of injection system. It can be clearly observed that a considerable percentage of angular momentum is lost, due to the physical existence of injection system up to r/D of 0.25. Even at 0.25 < r/D < 0.28 some angular momentum is lost within the injection-system boundary layer.

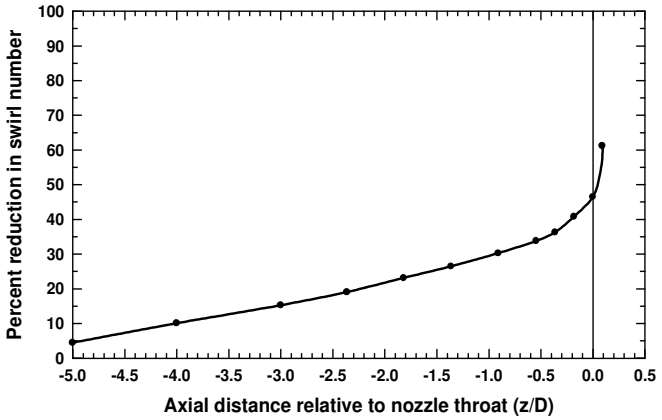

Figure 3. Relative reduction in subsonic swirl number due to presence of coaxial injection system. Nozzle throat at z/D = 0

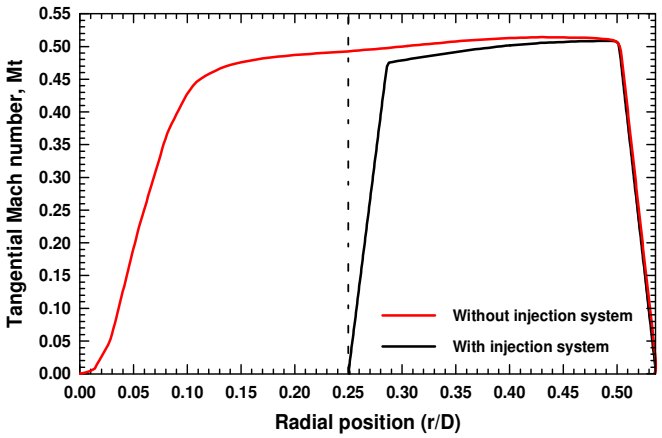

Figure 4. Radial variation of tangential Mach number at z/D of -0.1 in the absence (red) and presence (black, case 2) of injection system. Dotted line at r/D = 0.25 represents radius of coaxial injection system at tip

The combination of two facts is expected to induce these common observations of Figures 2 to 4. First, the angular momentum experiences higher losses, as the ratio of boundary-layer thickness to flow-passage height increases along the axial direction. Moreover, the injection system blocks higher percentages of nozzle cross-sectional area at downstream locations.

Nozzle Choking Criteria

Figure 5 examines the trans-throat flowfield by comparing the flow sections about nozzle throat (z/D = –0.1 and +0.1) in case 2. The radial variations of axial and tangential Mach number components (M_a and M_t) are shown in Figures 5a and 5b, respectively. A significant increase in trans-throat axial momentum is observed, which incorporates both jet acceleration and expansion. Significant radial expansion occurs in the absence of the restricting walls of nozzle and injection-system. On the other hand, a reduction in the magnitude of trans-throat M_t is observed, which agrees with the findings of Batson and Sforzini.[14] Figure 5b, however, reveals that radial expansion results in an increase in angular momentum, which is undermined by the decrease associated with the reduction in magnitude of M_t.

A notable observation to be made from Figure 5a is that the trans-throat magnitudes of M_a are subsonic in the swirling flowfield. This is distinctly different from the behavior of non-swirling flow, where M_a transitions to supersonic values through the throat. Figure 5c explains such unusual behavior under swirling conditions. Shown are the radial distributions of non-swirling and swirling trans-throat Mach number (M). The expected transition to supersonic propagation through nozzle throat is observed, which yields the main conclusion that non-swirling and swirling flowfields behave similarly in terms of M, and not M_a. Such similarity exists on both the qualitative and quantitative scales within the jet ($0.26 < r/D < 0.47$). Figure 6 further proves this fact by comparing the non-swirling and swirling sonic lines, which appear to be almost identical except at greater radii, where the sonic line is reached earlier in the swirling flowfield. This agrees again with the findings of Batson and Sforzini,[14] where it was reported that the flow velocity near the wall increases with swirl, due to Coriolis effects and area choking. The boundary layers are also identifiable in Figure 6 beyond the radial range $0.26 < r/D < 0.47$.

The remarkable similarity of trans-throat non-swirling and swirling flows can be traced back to the subsonic flowfield inside nozzle. Figure 7 shows the axial variations of cross-section-averaged subsonic Mach number. It is clearly noticeable how the non-swirling and swirling behaviors are almost identical, which strengthens the findings of Figure 5c. The axial variations of non-swirling and swirling, total and static temperatures inside nozzle are shown in Figure 8. Notice that the throat static temperature varies within a range of about 10 degrees only, which further proves the close similarity of non-swirling and swirling flowfields.

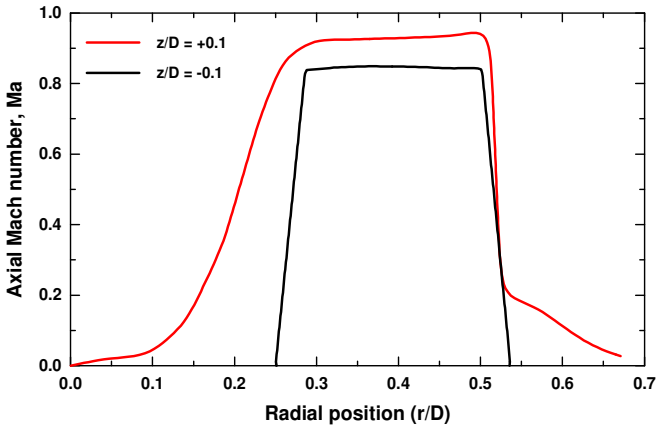

Figure 5a. Radial variation of trans-throat axial Mach-number (case 2)

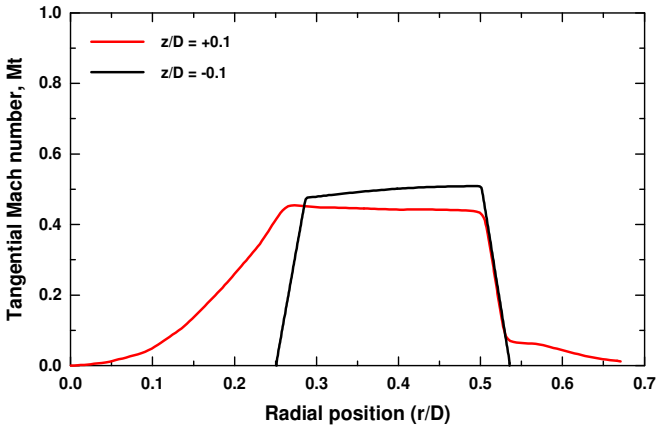

Figure 5b. Radial variation of trans-throat tangential Mach-number (case 2)

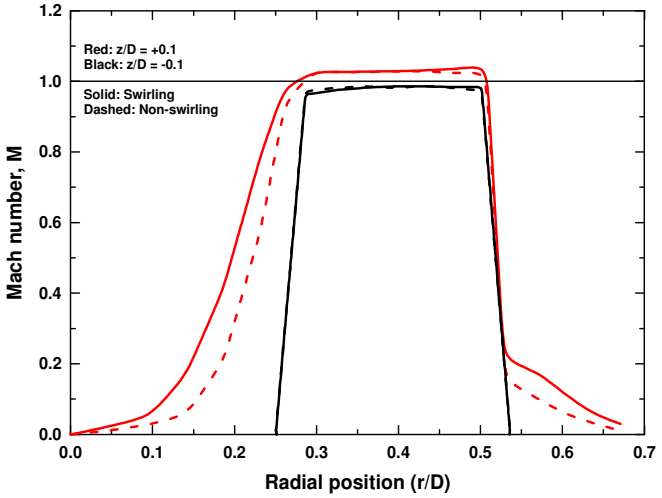

Figure 5c. Radial variations of trans-throat Mach number in cases 1 (non-swirling, dashed) and 2 (swirling, solid)

Downloaded by UNIVERSITY OF MARYLAND on September 7, 2014 | http://arc.aiaa.org | DOI: 10.2514/6.2009-5164

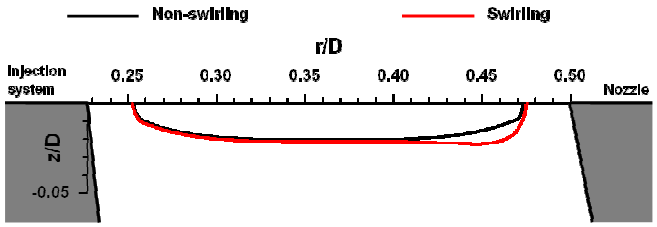

Figure 6. Sonic lines in cases 1 (non-swirling) and 2 (swirling)

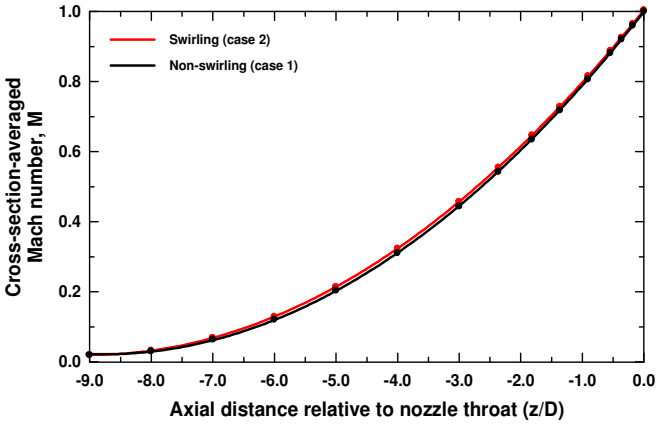

Figure 7. Axial variations of cross-section-averaged subsonic Mach number in cases 1 (non-swirling) and 2 (swirling)

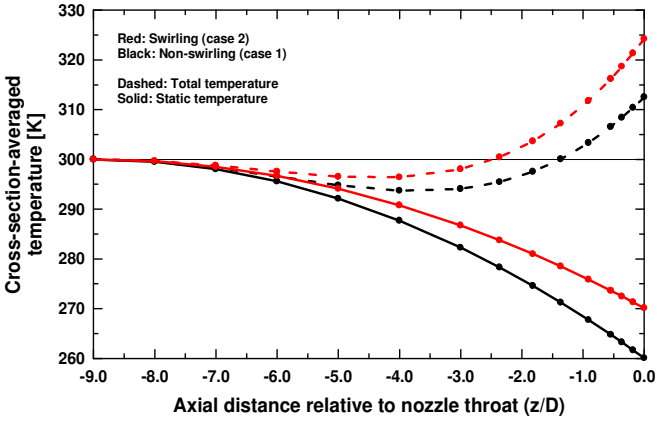

Figure 8. Axial variations of cross-section-averaged total and static temperatures inside nozzle in cases 1 (non-swirling, black) and 2 (swirling, red)

It should be noted at this point that the observed throat values of static temperature are considerably higher than what would be expected in isentropic flows. The isentropic value of sonic static temperature is 250 K in airflow of 300 K total temperature. This behavior can be explained by recalling that the nozzle examined here is made of aluminum. Its high thermal conductivity allows the nozzle to be almost isothermal at a temperature of about 280 K. The relatively warmer entrained ambient air loses heat to the external nozzle walls, which is conducted to the inner walls and convected to the flow within. The fact that the airflow inside nozzle is gaining heat energy (i.e., not isentropic) is evident in Figure 8, where it can be clearly observed that the throat total temperature is considerably higher than its 300-K inlet value. If the flow were isentropic, it would have a constant total temperature throughout.

Figure 8 also reveals that the total temperature initially decreases below 300 K by about 5 degrees in the upstream sections of nozzle before recovering and increasing beyond 300 K. This peculiar behavior can be explained by observing Figure 9, where a schematic representation of heat flow and static-temperature distribution is depicted. Notice that the static temperature of nozzle flow decreases from 300 K at inlet to about 265 K at throat. Meanwhile, the stagnation temperature of ambient air is 300 K, and the temperature of nozzle walls was found experimentally to be almost constant at 280 K. It is expected to observe heat transfer from the ambient air to nozzle flow at the downstream sections. The heat flux is expected to increase as the flow approaches nozzle throat, because (a) temperature difference between ambient air and nozzle flow increases, and (b) the thickness of nozzle wall decreases. In other words, the potential for heat transfer increases, while the resistance decreases. This explains the greater rates of total-temperature increase in Figure 8 as throat is approached. The peculiar observation, however, is that the 280-K nozzle walls are surrounded by warmer media on both sides at the upstream sections. This allows heat to be conducted axially downstream through the walls from both the ambient air and nozzle flow. The heat lost from the latter at the upstream sections explains the initial decrease in flow total temperature below 300 K, before recovery occurs at the downstream sections.

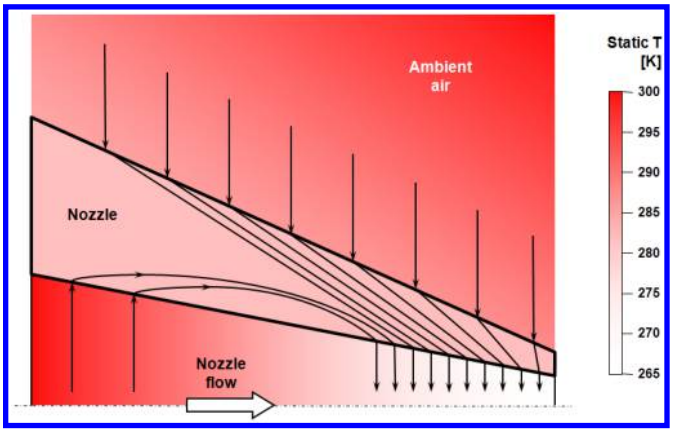

Figure 9. Schematic representation of heat flow and static-temperature distribution

Downloaded by UNIVERSITY OF MARYLAND on September 7, 2014 | http://arc.aiaa.org | DOI: 10.2514/6.2009-5164

Downloaded by UNIVERSITY OF MARYLAND on September 7, 2014 | http://arc.aiaa.org | DOI: 10.2514/6.2009-5164

It might be argued here that these examined conditions do not compare directly to the fundamental isentropic quasi-1D flow through nozzles, so how does the current analysis contribute to the understanding of the effect of swirl on such basic flow? The answer to this question is twofold. First, it was proven in the literature that 1-D approximation cannot be applied to swirling flows without either violating some conservation equations or enforcing assumptions that are too ideal for actual flows. Three-dimensional viscous numerical simulations, on the other hand, can now be implemented to study the behavior of such actual flows. Second, non-isentropic nozzle flows with heat transfer through nozzle walls occur in a number of important practical propulsion applications, including turbofans and turbojet engines, spin-stabilized rockets, and integral rocket/ramjets. Heat transfer is essential for cooling the nozzle walls, especially near the throat section. The presented distributions of Mach number, pressure, and temperature might be specific to the examined geometry, which is also the case in many previous studies. Nevertheless, this study contributes significantly to the understanding of the similarities and differences of non-swirling and swirling flows. No idealized assumptions are made, which would limit the applicability of the attained findings in engine/ nozzle design or numerical-model development.

Having observed that the throat static temperature varies within ~10 degrees with swirl, the question that arises here is whether this is the actual effect of swirl or the result of the swirling flow taking a longer path through the nozzle and thus getting heated up by the relatively warmer 280-K nozzle walls. The answer to this question is discussed as follows. Consider case 3, which is a swirling case like 2 but has the lower reservoir pressure of case 1. All three cases have the same inlet total temperature of 300 K. A side argument might be made here that the aforementioned Mach-number similarity of non-swirling and swirling flows is attributed to the higher nozzle reservoir pressure with swirl, which leads to a common air flow rate. Figure 10, however, refutes this argument. Shown are the axial variations of Mach number inside nozzle for cases 1, 2, and 3. It is clearly evident that non-swirling and swirling flows are unconditionally similar in terms of Mach number, regardless of inlet conditions.

In terms of temperature, on the other hand, it is expected here that only cases 2 and 3 will behave identically. Both are swirling, and the airflow takes the same longer path through nozzle in both. Figure 11, however, shows that the resemblance is only qualitative. Depicted are the axial variations of total and static temperatures inside nozzle for cases 1, 2, and 3. It can be distinctly seen that case 3 is identical to neither 1 nor 2. These differences are believed to be partially attributed to an implicit effect of total pressure. It is known that pressure is a form of energy, i.e., the higher the flow pressure is, the greater is its energy potential. This extra energy can be transformed to other forms within the flow, e.g., viscous heating. If case 3 is compared to 2 from this point of view, it can be deduced that the latter simply has more energy. Cases 1 and 3, on the other hand, start off with the same energy level (same inlet total temperature and pressure). The difference in static temperature between 1 and 3 can thus be mainly attributed to more heat gained by the latter from nozzle walls along its longer path inside nozzle.

Consequently, since cases 3 and 2 share the same longer path, the difference in static temperature between them cannot be attributed to heat transfer from nozzle walls. Part of the extra pressure energy stored within the 2-flow is believed to be consumed in viscous heating, since 175 g/s of air are forced through the nozzle, whereas case 3 has a lower flow rate of only 150 g/s. Therefore, the overall increase in total temperature from case 1 to 2 incorporates both external heating through nozzle walls (≈ 60% in this study) and internal viscous heating through the transformation of some pressure energy into heat (≈ 40%).

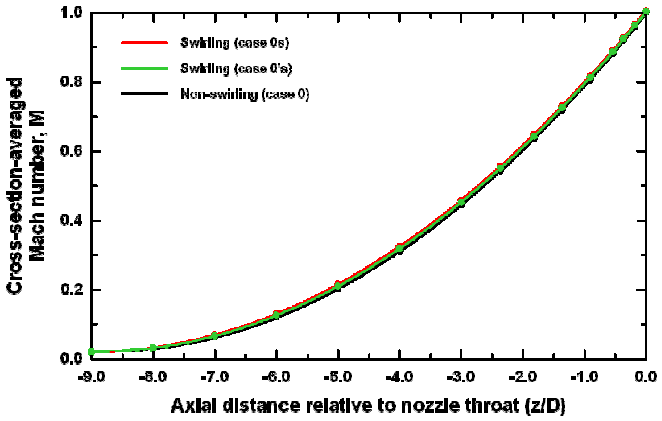

Figure 10. Axial variations of cross-section-averaged subsonic Mach number in cases 1 (non-swirling, reservoir pressure = 7.91 bar), 2 (swirling, reservoir pressure = 8.82 bar), and 3 (swirling, reservoir pressure = 7.91 bar)

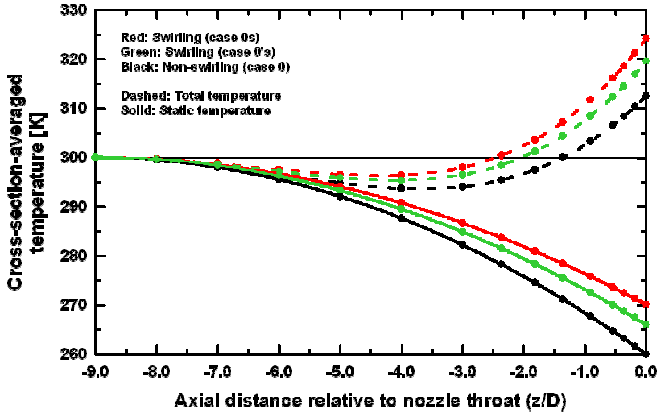

Figure 11. Axial variations of cross-section-averaged total and static temperatures inside nozzle in cases 1 (non-swirling, reservoir pressure = 7.91 bar), 2 (swirling, reservoir pressure = 8.82 bar), and 3 (swirling, reservoir pressure = 7.91 bar)

Having analyzed the Mach number and total and static temperatures, the discussion proceeds to analyzing the effect of swirl on the total and static pressures. Figure 12 shows the subsonic axial variations of total and static pressures for cases 1, 2, and 3. The first important observation to be made is that no significant pressure energy is consumed in additional viscous heating when case 1 is swirled to become case 3. This confirms the aforementioned argument that the difference in static temperature between 1 and 3 is attributed mainly to more heat gained by the latter from nozzle walls. A fundamental question arises at this point: If the application of swirl at the same nozzle reservoir pressure (i.e., cases 1 and 3) results in very minor changes in throat static pressure and temperature, then what causes the significant reduction in flow rate with swirl? Recall that the mass flow rate is the product of throat density, cross-sectional area, and axial velocity component, i.e.,

$$\dot{m} = \left(\rho A v_a\right)_{throat} = \left(\frac{p}{RT} A M_a \sqrt{\gamma R T}\right)_{throat}$$

If the minor changes in throat static temperature are neglected, the above equation reduces to

$$\dot{m} \propto \left(p M_a\right)_{throat}$$

Recall from the analyses of Figures 5a, 5c, and 10 that non-swirling and swirling flows are similar in terms of overall Mach number (M) and not axial Mach number component (M_a). At the throat, $M_a = M = 1$ in non-swirling flows, but $M_a < M = 1$ in the swirling ones. Therefore, swirl results in a reduction in axial Mach number component. If no measures are taken towards increasing the nozzle reservoir pressure (cases 1 and 3), the throat static pressure remains almost unchanged (Figure 12), and the preceding equation dictates that the mass flow rate will decrease. The greater reservoir pressure of case 2, on the other hand, results in a higher throat static pressure, which compensates for the reduced axial Mach number component with swirl, and the mass flow rate can thus be matched to its non-swirling value. This explains the need for higher nozzle reservoir pressure with swirl to avoid reduction in mass flow rate.

The analysis of nozzle flowfield is concluded here by a remark that pertains to the tangential component of Mach number, M_t. It has been observed that the limiting Mach number in a swirling flowfield is the overall Mach number. It reaches its sonic value at the throat, independent of flow rate and inlet conditions, which means that all three components of Mach number are intrinsically subsonic. At extremely high degrees of swirl the value of tangential component approaches that of overall Mach number, which is believed to remain sonic at the throat. It should be noted here that this could not be examined experimentally in this study. No numerical simulations were conducted either in this regard, as they would not be considered a solid reference in the absence of experimental validation. Nevertheless, the current findings of this study support those of Toomre[12] and

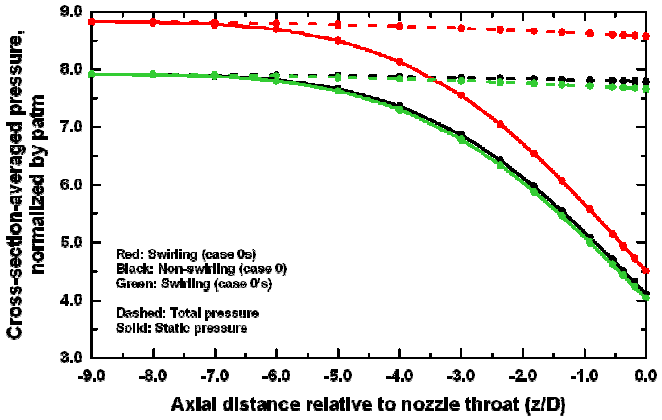

Figure 12. Axial variations of cross-section-averaged total and static pressures inside nozzle in cases 1 (non-swirling, reservoir pressure = 7.91 bar), 2 (swirling, reservoir pressure = 8.82 bar), and 3 (swirling, reservoir pressure = 7.91 bar)

Roschke and Pivirotto,[11] where it was reported that the limiting tangential Mach number is almost unity. The findings of Lewellen et al.[10] and Pinchak and Poplawski,[13] who reported values of 1.2 and 1.18, respectively, are, however, questioned here but not refuted.

Supersonic Propagation of Swirl

Figure 13 shows the near-field axial variation of supersonic swirl number in case 2. It decreases in the axial direction, which is again attributed to substantial increase in axial momentum, as the flow expands and accelerates. A minimum swirl number of 0.07 is observed at z/D of ~1.4. The swirl number then experiences a slight local increase between z/D of 1.4 and 2.7, which is attributed to the effect of shock structure.[23] To understand why the supersonic swirl number experiences a slight local increase within the shock structure, it should be noted that the axial and tangential velocity components behave very differently through shock waves. Figure 14 helps explain this statement. Depicted is a three-dimensional schematic of shock structure, showing the orientation of v_a and v_t with respect to the main features, i.e., Mach disk, intercepting, and reflected shocks. It can be easily visualized how v_a is always perpendicular to the Mach disk. Moreover, both intercepting and reflected shocks are oblique with respect to v_a. For these two reasons, the axial Mach number and momentum undergo significant reductions through shock structure. The tangential velocity component, on the other hand, is always parallel to all features of shock structure. According to the fundamentals of gas dynamics, the velocity component parallel to the plane of a shock wave is preserved through the shock and experiences no change. Combining the behaviors of v_a and v_t, one can easily explain the small local increase in swirl number within the realm of shock structure, especially when one recalls that the swirl number is approximately proportional to the ratio of average tangential to axial momenta.

Downloaded by UNIVERSITY OF MARYLAND on September 7, 2014 | http://arc.aiaa.org | DOI: 10.2514/6.2009-5164

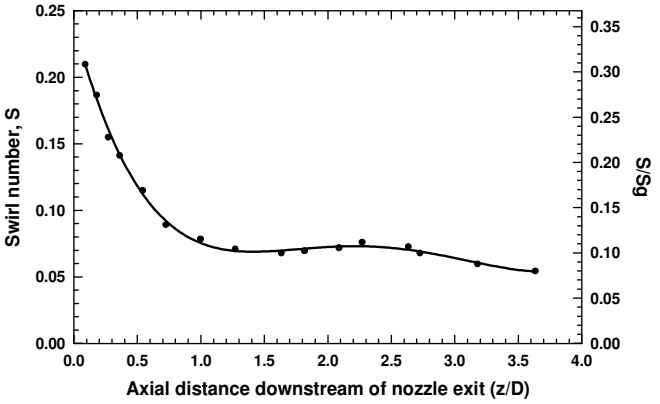

Figure 13. Near-field axial variation of supersonic swirl number in case 2

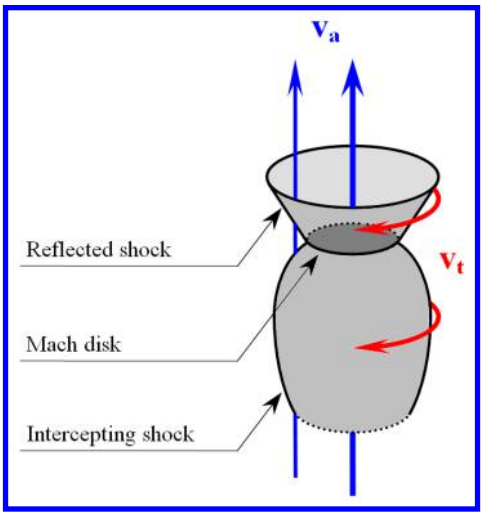

Figure 14. Three-dimensional schematic of shock structure showing orientation of axial and tangential velocity components with respect to Mach disk and intercepting and reflected shocks

VI. Conclusions

The propagation of swirl and the choking criteria of swirling transonic airflow have been examined both numerically and experimentally in underexpanded airflow at matched nozzle reservoir pressure as well as matched mass flow. The following conclusions were made: (a) The swirl number is not conserved in the expanding subsonic flowfield inside nozzle but decreases as the throat is approached. (b) The throat velocity itself (not any of its components) is choked in a swirling flowfield. Therefore, the limiting tangential Mach number is unity. Moreover, the application of swirl always results in a reduction in axial Mach number component. (c) The mass flow rate through nozzle is a function of throat density and axial Mach number. The reduction in the latter with swirl explains the observed reduction in mass flow (discharge coefficient) at matched nozzle reservoir pressure. Greater reservoir pressures, on the other hand, result in higher throat densities, which compensates for the reduced axial Mach number, and the mass flow rate can be kept constant at its non-swirling value. (d) The distribution of subsonic Mach number (not any of its components) in a swirling flow is solely dependent on cross-sectional area, similar to non-swirling flows, i.e., non-swirling and swirling flows have the same subsonic Mach number profile. (e) The supersonic swirl number experiences a slight local increase within shock structure, where the axial momentum undergoes significant reduction, whereas the tangential one is preserved and experiences no change.

Acknowledgments

This work was supported by the Space Vehicle Technology Institute, jointly funded by NASA, DoD, and USAF within the NASA Constellation University Institutes Project (CUIP), with Claudia Meyer as the Project Manager. This support is gratefully acknowledged.

The simulation package CFD-GEOM, CFD-FASTRAN, and CFD-VIEW was provided by ESI-Group and CFDRC. This support is gratefully acknowledged.

References

[1]Buckley, P. L., Craig, R. R., Davis, D. L., and Schwartzkopf, K. G., "The Design and Combustion Performance of Practical Swirlers for Integral Rocket/ Ramjets," AIAA Journal, Vol. 21, No. 5, 1983, pp. 733-740.

[2]Mager, A., "Approximate Solution of Isentropic Swirling Flow through a Nozzle," ARS Journal, Vol. 31, No. 8, 1961, pp. 1140-1148.

[3]Swithenbank, J. and Sotter, G., "Vortex Generation in Solid Propellant Rockets," AIAA Journal, Vol. 2, No. 7, 1964, pp. 1297-1302.

[4]Glick, R. L. and Kilgore, M. S., "Effect of Specific-Heat Ratio on Mass Flow for Swirling Nozzle Flow," Journal of Spacecraft and Rockets, Vol. 4, No. 8, 1967, pp. 1098-1099.

[5]Bastress, E. K., "Interior Ballistics of Spinning Solid-Propellant Rockets," Journal of Spacecraft and Rockets, Vol. 2, No. 3, 1965, pp. 455-457.

[6]Manda, L. J., "Spin Effects on Rocket Nozzle Performance," Journal of Spacecraft and Rockets, Vol. 3, No. 11, 1966, pp. 1695-1696.

[7]King, M. K., Comment on "Spin Effects on Rocket Nozzle Performance," Journal of Spacecraft and Rockets, Vol. 3, No. 12, 1966, pp. 1812-1813.

[8]Manda, L. J., Reply by author to M. K. King, Journal of Spacecraft and Rockets, Vol. 3, No. 12, 1966, p. 1813.

[9]Hsu, C., "Mass Blocking of Swirling Flow in Nozzles," Journal of Spacecraft and Rockets, Vol. 8, No. 12, 1971, pp. 1232-1234.

Downloaded by UNIVERSITY OF MARYLAND on September 7, 2014 | http://arc.aiaa.org | DOI: 10.2514/6.2009-5164

[10]Lewellen, W. S., Burns, W. J., and Strickland, H. J., "Transonic Swirling Flow," AIAA Journal, Vol. 7, No. 7, July, 1969, pp. 1290-1297.

[11]Roschke, E. J. and Pivirotto, T. J., "Similarity in Confined Vortex Flows," Technical Report 32-789, 1965, Jet Propulsion Laboratory.

[12]Toomre, J., "Highly Swirling Flows Through a Convergent-Divergent Nozzle," MSc thesis, Massachusetts Institute of Technology, Cambridge, MA, June 1963.

[13]Pinchak, A. C. and Poplawski, R., "On the Attainment of Extremely High Rotational Velocities in a Confined Vortex Flow," 2nd AIAA Annual Meeting, San Francisco, CA, July 26-29, 1965, AIAA-65-400.

[14]Batson, J. L. and Sforzini, R. H., "Swirling Flow through a Nozzle," Journal of Spacecraft and Rockets, Vol. 7, No. 2, 1970, pp. 159-163.

[15]Kornblum, B. T., Thompson, H. D., and Hoffman, J. D., "An Analytical Investigation of Swirl in Annular Propulsive Nozzles," Journal of Propulsion and Power, Vol. 2, No. 2, 1986, pp. 155-160.

[16]Hoffman, J. D., Thompson, H. D., and Marcum, D. L., "Analytical Study of Swirler Effects in Annular Propulsive Nozzles," Journal of Propulsion and Power, Vol. 3, No. 5, 1987, pp. 465-466.

[17]Gupta, A. K., Lilley, D. G., and Syred, N., "Swirl Flows," Abacus Press, UK, 1984, ISBN 0-85626-175-0.

[18]Cutler, A. D., Levey, B. S., and Kraus, D. K., "Near-Field Flow of Supersonic Swirling Jets," AIAA Journal, Vol. 33, No. 5, 1995, pp. 876–881.

[19]Linck, M., "Spray Flame and Exhaust Jet Characteristics of a Pressurized Swirl Combustor," PhD thesis, University of Maryland, College Park, MD, May 2006.

[20]Baldwin, B. S. and Lomax, H., "Thin Layer Approximation and Algebraic Model for Separated Turbulent Flows," 16th AIAA Aerospace Sciences Meeting, Huntsville, Alabama, Jan. 16-18, 1978, AIAA-78-257.

[21]Courant, R., Friedrichs, K., and Lewy, H., "On the Partial Difference Equations of Mathematical Physics," IBM Journal, Vol. 11, Mar. 1967, pp. 215-234.

[22]Lee, K. H., Setoguchi, T., Matsuo, S., and Kim, H. D., "Influence of the Nozzle Inlet Configuration on Underexpanded Swirling Jet," Proceedings of the Institution of Mechanical Engineers, Part C: Journal of Mechanical Engineering Science, Vol. 220, No. 2, 2006, pp. 155-163.

[23]Abdelhafez, A. and Gupta, A. K., "Swirl Effects on Shock Structure in Free Under-Expanded Supersonic-Nozzle Airflow," 44th AIAA/ASME/SAE/ASEE Joint Propulsion Conference and Exhibit, Hartford, CT, July 21-23, 2008, AIAA-2008-4502.

Downloaded by UNIVERSITY OF MARYLAND on September 7, 2014 | http://arc.aiaa.org | DOI: 10.2514/6.2009-5164

This article has been cited by:

1. N. Bellomo, F. Barato, M. Faenza, M. Lazzarin, A. Bettella, D. Pavarin. 2013. Numerical and Experimental Investigation of Unidirectional Vortex Injection in Hybrid Rocket Engines. *Journal of Propulsion and Power* **29**:5, 1097-1113. [Abstract] [Full Text] [PDF] [PDF Plus]

Downloaded by UNIVERSITY OF MARYLAND on September 7, 2014 | http://arc.aiaa.org | DOI: 10.2514/6.2009-5164